Resonance Raman Analysis of Chromophore Structure in the Lumi-R Photoproduct of Phytochrome†

Frank Andel III,‡ J. Clark Lagarias,§ and Richard A. Mathies*,‡

Department of Chemistry, University of California, Berkeley, California 94720, and Section of Molecular and Cell Biology, University of California, Davis, California 95616

Received August 27, 1996; Revised Manuscript Received October 9, 1996⊗

ABSTRACT: Resonance Raman vibrational spectra of the P_r, lumi-R, and P_{fr} forms of phytochrome have been obtained using low-temperature trapping and room temperature flow techniques in conjunction with shifted-excitation Raman difference spectroscopy (SERDS). The P_r to lumi-R photoconversion exhibits a thermal barrier and is completely blocked at 30 K, indicating that thermally assisted protein relaxation is necessary for the primary photochemistry. When P_r is converted to lumi-R, new bands appear in the C=C and C=N stretching regions at 1651, 1636, 1590, and 1569 cm^{-1}, indicating that a significant structural change of the chromophore has occurred. The photoconversion also results in an 18 cm^{-1} decrease in the N−H rocking band in lumi-R. Normal mode calculations correlate this frequency drop with a change in the geometry of the C_{15} methine bridge of the phytochromobilin chromophore. Additionally, a C=N stretching mode marker band shifts from 1576 cm^{-1} in P_r to 1569 cm^{-1} in lumi-R and to 1552 cm^{-1} in P_{fr}. Normal mode calculations show that the frequency drop of this band in the lumi-R → P_{fr} interconversion is an indication of a C_{14}−C_{15} *syn* → *anti* conformational change. Moderately intense hydrogen out-of-plane modes that occur at 805 cm^{-1} in P_r shift to 829 and 847 cm^{-1} upon photoconversion to lumi-R and are replaced by a very intense mode at 814 cm^{-1} in P_{fr}. These observations indicate that the C and D rings of the chromophore in P_r and lumi-R are moderately planar but that they become highly distorted in P_{fr}. This information suggests that the primary photochemistry in phytochrome is a *Z* → *E* isomerization of the C_{15}=C_{16} bond of P_r giving lumi-R. This is followed by a thermal *syn* → *anti* C_{14}−C_{15} conformational relaxation to form P_{fr}. A four-state model is presented to explain the chromophore structural changes in P_r, lumi-R, and P_{fr} that uses hydrogen bonding to the surrounding protein to stabilize the high-energy P_{fr} C_{15}=C_{16}, C_{14}−C_{15}, *E,anti* chromphore structure. This implicates an anchor and release mechanism between the chromophore and protein that might lead to altered biological signaling in the plant.

Plants detect the quality and quantity of light in their environment and use this information to adapt patterns of growth and development to their surroundings (Kendrick & Kronenberg, 1994). These processes, collectively termed photomorphogenesis, are controlled by several photoreceptors including the biliprotein phytochrome (Pratt, 1995). Phytochrome isolated from etiolated oat seedlings (*Avena sativa*) is a water-soluble protein which consists of two 124 kDa subunits (Vierstra & Quail, 1986). Each subunit contains a thioether-linked 2,3-dihydrobiliverdin prosthetic group called phytochromobilin (Lagarias & Rapoport, 1980). Phytochrome exists in one of two photointerconvertible forms: P_r,[1] which absorbs light in the red (550−700 nm) region of the visible spectrum, and P_{fr}, which absorbs light in the far-red region (600−800 nm). The incident light controls the steady-state ratio of P_r/P_{fr} and hence the plant response via a molecular mechanism that is the subject of much exploration (Bowler et al., 1994; Elich & Chory, 1994; Quail et al., 1995).

A number of spectrophotometrically identifiable intermediates accompany the P_r → P_{fr} transformation and have been detected using time-resolved and low-temperature trapping techniques (Figure 1). Photoexcitation of P_r produces a primary photoproduct absorbing near 700 nm called lumi-R which decays on a microsecond time scale to meta-R_a, followed by several other meta intermediates which appear and decay in the microsecond to millisecond time domain (Bjorling et al., 1992; Rudiger, 1992; Zhang et al., 1992). The back-reaction from P_{fr} to P_r also proceeds through at least three spectrally distinct intermediates which have recently been further characterized (Chen et al., 1996).

The structure and protonation state of the phytochrome chromophore have been examined by a variety of techniques (Rudiger, 1992; Song, 1988). On the basis of ^{1}H NMR studies of chromopeptides, Rudiger et al. (1983) proposed that the conversion from P_r to P_{fr} involves a photochemical *Z* → *E* isomerization of the tetrapyrrole at the C_{15}−methine bridge. Recently, FT Raman spectra of the intermediates lumi-R, lumi-F, and meta-F using low-temperature trapping techniques have been interpreted to support the hypothesis

† This work was supported by NSF Grants CHE 94-19714 to R.A.M. and MCB92-06110 to J.C.L.

* Author to whom correspondence should be addressed.

‡ University of California, Berkeley.

§ University of California, Davis.

⊗ Abstract published in *Advance ACS Abstracts,* December 1, 1996.

[1] Abbreviations: CCD, charge-coupled device; EDTA, ethylenediaminetetraacetate; EGTA, ethylene glycol bis(β-aminoethyl ether); EPPS, *N*-(2-hydroxyethyl)piperazine-*N*′-3-propanesulfonic acid; P_r, the red light absorbing form of phytochrome; P_{fr}, the far-red light absorbing form of phytochrome; PEI, poly(ethylenimine); PMSF, phenylmethanesulfonyl fluoride; QCFF, quantum chemistry force field; SERDS, shifted-excitation Raman difference spectroscopy.

S0006-2960(96)02175-7 CCC: $12.00

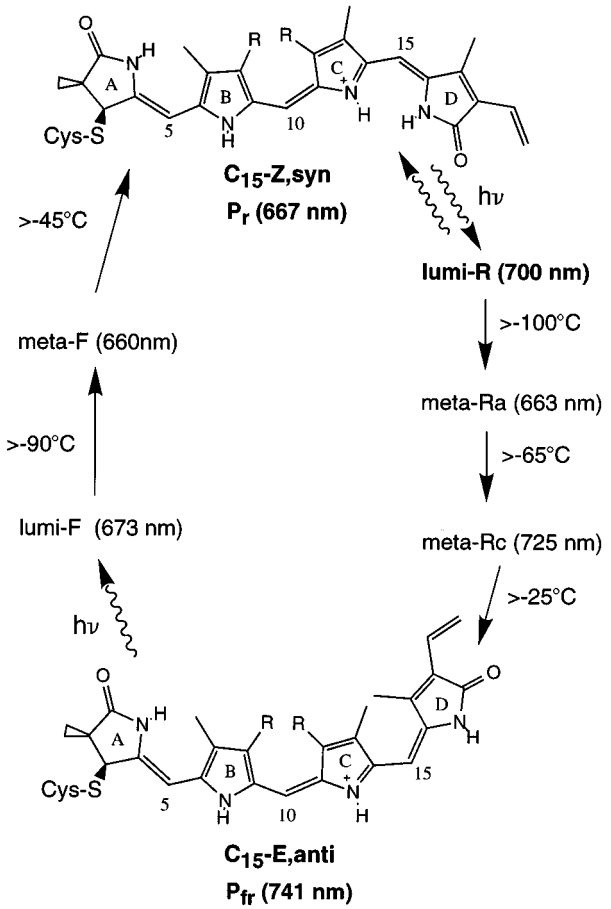

FIGURE 1: Photocycle of phytochrome showing the C_5-*Z,anti*, C_{10}-*E,anti*, C_{15}-*Z,syn* chromophore geometry for P_r and the C_5-*Z,anti*, C_{10}-*E,anti*, C_{15}-*E,anti* chromophore geometry for P_{fr} where R = $CH_2CH_2CO_2^-$. Also shown are the wavelength maxima of the intermediates and the temperatures at which the thermal transitions are blocked.

that the $P_r \rightarrow$ lumi-R photoconversion encompasses a double bond isomerization and torsional changes about two exocyclic single bonds (Matysik et al., 1995). These investigators further concluded that the chromophore is fully protonated in both P_r and lumi-R. Mizutani et al. (1994) proposed that chromophore deprotonation occurs after the $P_r \rightarrow$ lumi-R transition, forming a species called I_{bl}, and that the chromophore is deprotonated in P_{fr}.

We have been examining chromophore structure in phytochrome with resonance Raman spectroscopy because it is a sensitive *in situ* structural probe. Initial application of this technique to phytochrome was inhibited by the intrinsic fluorescence of this protein for which the quantum yield is $\sim 10^{-3}$ (Brock et al., 1987). Raman spectra of phytochrome have been previously obtained using methods such as preresonant excitation (Fodor et al., 1988, 1990), Fourier transform Raman spectroscopy (Hildebrandt et al., 1992), surface-enhanced resonance Raman spectroscopy (Farrens et al., 1989; Holt et al., 1989), and Soret band excitation (Tokutomi et al., 1990; Mizutani et al., 1991, 1994). Although the consensus of these studies is that the geometry of the methine bridge between the phytochromobilin C and D rings is C_{15}═C_{16},*Z* in P_r and C_{15}═C_{16},*E* in P_{fr}, the nature of the primary photochemistry and the structure of the chromophore in the various intermediates in this reaction pathway have not been elucidated.

Here, we report resonance Raman spectra of lumi-R, the photoreversible primary photoproduct of P_r. Low-temperature trapping was used to prevent P_r conversion from proceeding beyond the primary photoproduct. The 750 nm excitation wavelength used is sufficiently red to avoid photoconversion of lumi-R back to P_r and to reduce fluorescence background emission, while still providing resonance enhancement of lumi-R Raman scattering. When P_r is converted to lumi-R, significant changes are observed in the C═C and C═NH stretching, N−H rocking, and C−H wagging regions of the resonance Raman spectra that are analyzed through comparison with normal mode calculations and isotopic substitution. These spectra provide us with new information concerning the structural differences and protonation states of the chromophore in P_r, lumi-R, and P_{fr} chromophores. This information has enabled us to examine whether the $P_r \rightarrow P_{fr}$ interconversion involves concerted photochemical C═C and C−C bond isomerization or sequential rotations about the C═C and C−C bonds.

MATERIALS AND METHODS

Sample Preparation. Phytochrome was purified according to the method of Grimm and Rudiger (1986) with the following modifications. Etiolated oat seedlings (5 days old, 2 kg) were homogenized with 1.5 L of extraction buffer [100 mM Tris-HCl, pH 8.3, 200 mM $(NH_4)_2SO_4$, 2 mM ethylenediaminetetraacetate (EDTA), 2 mM ethylene glycol bis-(β-aminoethyl ether) (EGTA), 285 mM 2-mercaptoethanol, 50% (v/v) ethylene glycol, and 4 mM phenylmethanesulfonyl fluoride (PMSF)] in a Waring blender. The crude homogenate was filtered through cheesecloth on ice and 40 mL of 10% poly(ethylenimine) (PEI) solution was added per liter of extract. After being stirred for 15 min, the mixture was centrifuged for 30 min at 12 500 rpm in a GS3 rotor and the supernatant collected.

The phytochrome-containing supernatant was converted to the P_{fr} form by irradiation with 660 nm light for 15 min on ice. PMSF (1.0 g), dissolved in 20 mL of absolute ethanol, was added to the solution, and 250 g of ammonium sulfate was slowly added per liter of extract. After being stirred for 60 min, the suspension was centrifuged for 30 min at 27 000 rpm in a GS3 rotor. Protein pellets were dissolved in resolubilization buffer (4.5 mL/phytochrome unit) consisting of 25% (v/v) ethylene glycol, 50 mM Tris-HCl, pH 7.8, 5 mM Na_4EDTA, 14 mM 2-mercaptoethanol, and 2 mM PMSF. The solution was clarified by centrifugation at 12 500 rpm for 20 min in a GS3 rotor.

The clarified solution was loaded onto a hydroxylapatite column (4.5 × 8 cm) preequilibrated with the resolubilization buffer supplemented with 70 mM ammonium sulfate. The column was then washed with 500 mL of wash buffer consisting of 50 mM Tris-HCl, pH 7.8, 5 mM Na_4EDTA, and 14 mM 2-mercaptoethanol. A linear gradient using two phosphate buffers (5 mM and 200 mM phosphate, pH = 7.8) each containing 5 mM EDTA and 14 mM 2-mercaptoethanol was used to elute phytochrome from the column. Fractions which contained phytochrome ($A_{667nm} > 0.08$ in the P_{fr} form) were pooled, and ammonium sulfate was added to give a 42% (w/v) saturated solution. The mixture was stirred for 30 min and then centrifuged at 46 000 rpm for 20 min.

Pellets containing phytochrome were further purified using two salt washes. First, pellets were washed with a 10 mM

phosphate buffer (0.65 mL/phytochrome unit, pH 7.8, containing 5 mM EDTA and 14 mM 2-mercaptoethanol) with stirring for 20 min. The mixture was centrifuged for 20 min at 46 000 rpm and the supernatant discarded. The pellet was further washed with a 100 mM phosphate buffer (0.85 mL/phytochrome unit, pH 7.8, containing 5 mM EDTA and 14 mM 2-mercaptoethanol). After being stirred for 20 min, the mixture was spun at 46 000 rpm for 20 min. The remaining phytochrome-containing pellets were dissolved in 10 mM phosphate buffer (0.9 mL/phytochrome unit) and dialyzed against the desired spectroscopic solvent. For samples in D_2O, the phytochrome was photocycled in white light for 3−5 min to ensure complete isotope exchange. Typically, samples had a specific absorbance ratio (SAR = A_{667nm}/A_{260nm} for the P_r form) above 0.7.

Resonance Raman Spectra. To obtain resonance Raman spectra of P_r and lumi-R, both a Harney−Miller cell (Miller & Harney, 1970) and He-cooled cryostat (CTI-cryogenics, Model 21) were used. For Harney−Miller cell experiments, a capillary containing 75 μM (9.3 mg/mL) phytochrome in 50 mM *N*-(2-hydroxyethyl)piperazine-*N*′-3-propanesulfonic acid (EPPS), pH 8.0, buffer and 1 mM EDTA was suspended in the vacuum-jacketed glass cell. The room temperature sample was first illuminated with 15 mW of 750 nm light to convert it completely to the P_r form, allowed to relax in the dark for several minutes, and then cooled rapidly in the dark to 150 K with a stream of nitrogen gas that had passed through a liquid nitrogen reservoir. To convert P_r to lumi-R, the sample was illuminated with approximately 40 mW of 647 nm light from a Kr^+ laser for 10 min, which produced a steady-state mixture of both species. A 15 mW 750 nm probe beam of cylindrically focused (fl = 75 mm) light was used to obtain a resonance Raman spectrum of P_r before 647 nm illumination and of the steady-state mixture of P_r and lumi-R after 647 nm illumination. The spectrum of lumi-R was obtained by subtraction. For the experiments using the He-cooled cryostat, a small sample of phytochrome was applied to a copper tip attached to the cooling stage of the instrument. Conversion of the sample to P_r prior to cooling and conversion to lumi-R were performed as in the Harney−Miller cell experiments. The pD of the D_2O buffers was adjusted using pD = pH + 0.4. The 90° scattered light was detected with a cryogenically cooled CCD detector (LN/CCD-1152, Princeton Instruments) coupled to a subtractive-dispersion, double spectrograph (Mathies & Yu, 1978). Raman spectra were corrected for the spectral sensitivity of the detection system using a standard quartz tungsten halogen lamp (EG&G, Model 590−20) and frequency calibrated with a neon emission lamp.

For the P_{fr} experiments, phytochrome was dissolved in a 50 mM EPPS, pH 8.0, buffer containing 1 mM EDTA to give a concentration of 15 μM (1.9 mg/mL) and a final optical density of 2/cm (P_r form) at 666 nm. Five milliliters of this solution was placed in a closed-loop recirculating flow system consisting of silicone tubing attached to a 1 mm i.d. glass capillary and a reservoir. The room temperature sample was circulated with a Cole−Parmer Model 7535−20 peristaltic pump at a linear velocity of 35 cm/s. The reservoir was illuminated with 30 mW of 647 nm light from a Kr^+ laser to convert and maintain the sample in the P_{fr} form. Raman spectra were acquired by illuminating the P_{fr} molecules with 15 mW of cylindrically focused, 750 nm light (fl = 75 mm) from a Ti:sapphire laser as they flowed through the capillary. The dwell time between leaving the illuminated reservoir and arriving at the probe beam was about 1 s. This was sufficiently long to permit intermediates produced by the 647 nm actinic illumination to decay to P_r or P_{fr} (Bjorling et al., 1992; Zhang et al., 1992). Since the probe laser strongly overlaps with the P_{fr} absorption band, this method provides strong resonance enhancement of the scattering from P_{fr}. The back-conversion of P_{fr} to P_r by this probe beam depends on the photoalteration parameter, $F = (3.824 \times 10^{-21})P\epsilon\phi/\nu d$ (Mathies et al., 1976), where P is the laser power (photons/s), ϵ is the molar absorption coefficient (M^{-1} cm^{-1}), ϕ is the quantum yield for the photochemical reaction, ν is the flow velocity (cm/s), and d is the focused beam diameter (cm). For P_{fr}, $\epsilon_{750} = 57000$ M^{-1} cm^{-1}, $\phi = 0.069$ (Lagarias et al., 1987), and d is 0.5 cm, giving $F = 0.05$. This means that 5% of the P_{fr} molecules that flow through the probe laser beam will be photoconverted to P_r. Given the strong resonance enhancement of P_{fr} scattering over preresonant P_r with 750 nm excitation, these spectra should predominately consist of scattering from P_{fr} (>99%).

Resonance Raman spectra were acquired using the shifted-excitation Raman difference spectroscopy (SERDS) technique (Shreve et al., 1991, 1992) because it facilitates Raman spectral acquisition when there is a strong fluorescence background. With this technique, two Raman spectra are obtained with excitation frequencies shifted by 10 cm^{-1} relative to one another but with all other experimental conditions identical. The difference of these two spectra yields a SERDS spectrum. Derivative-like features, corresponding to Raman lines, are then fit to a model which assumes that the bands in the Raman spectrum are a difference of Gaussian peaks. The amplitude, position, and width of each peak are determined via nonlinear least-squares fit, and these parameters are then used to generate the Gaussian peaks representing the Raman spectrum. This method has been successfully applied to photosynthetic reaction centers, providing high quality, accurate resonance Raman spectra despite strong intrinsic fluorescence interference (Cherepy et al., 1994, 1995).

Vibrational Calculations. Vibrational calculations were performed on the phytochrome chromophore to aid in the interpretation of the Raman spectra. To simplify computation of vibrational modes, the propionate side chains and cysteine linkage of the phytochromobilin chromophore were substituted with methyl groups. Vibrational calculations were performed for the four possible structural isomers which may be obtained by rotating about the $C_{14}-C_{15}$ single or $C_{15}=C_{16}$ double bonds. These are the $C_{15}=C_{16}$, $C_{14}-C_{15}$, *Z,syn*, *Z,anti*, *E,syn*, and *E,anti* isomers. The remaining configurations and conformations about the C_5 and C_{10} exocyclic carbons were $C_4=C_5$, C_5-C_6, *Z,anti* and $C_{10}=C_{11}$, C_9-C_{10}, *E,anti* for all four isomers. The chromophore used in these calculations was fully protonated on all four pyrrolenic/lactam nitrogens. The geometries were minimized and the vibrations and intensities calculated according to the QCFF-π method (Warshel & Karplus, 1974). The intensities were calculated in the short time scattering limit as being proportional to $\Delta^2\omega^2$, where Δ is the change in the excited-state geometry for mode of frequency ω (Myers & Mathies, 1987). This method has been successfully used for modeling Raman intensities of rhodopsin (Kochendoerfer et al., 1996).

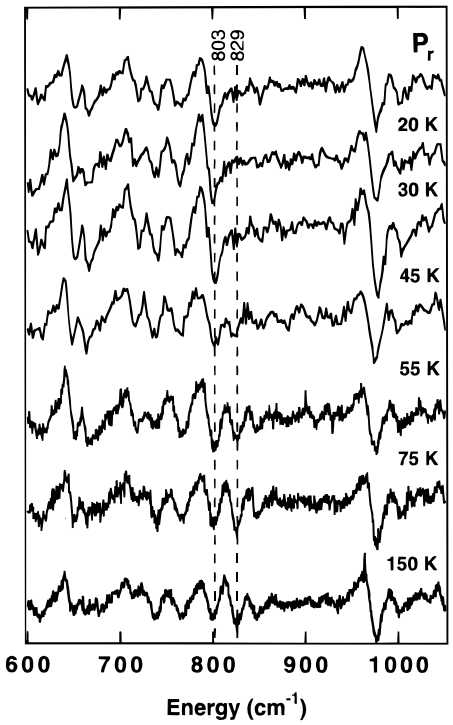

FIGURE 2: Shifted-excitation Raman difference spectra (SERDS) of P_r and the steady-state mixture of P_r and lumi-R formed after irradiation with 30 mW of 647 nm actinic light for 20 min at the indicated temperature. Spectra were acquired with 15 mW of 750 nm light after recooling to 20 K.

RESULTS

Determination of the Lumi-R Spectrum. To determine the structure of the chromophore in the lumi-R intermediate of phytochrome, it was first necessary to find conditions for observing its Raman spectrum and verifying that we were obtaining the Raman spectrum of the primary photoproduct of P_r. Figure 2 presents shifted-excitation Raman difference spectra (SERDS) of phytochrome obtained using a 750 nm probe beam. At 20 K, SERDS peaks are observed at 653, 668, 722, 765, and 805 cm^{-1} that are characteristic of the P_r chromophore (Fodor et al., 1988, 1990; Matysik et al., 1995). The phytochrome sample was then illuminated with 30 mW of 647 nm light from a Kr^+ laser for 20 min at the specified temperature to convert P_r to the lumi-R species. The sample was then recooled to 20 K, and spectra were obtained with the 750 nm probe beam which is sufficiently red that it does not alter the populations of the various intermediates during data acquisition.

Actinic pumping with 647 nm light at 20 and 30 K for periods as long as 1 h produces a spectrum that is identical to that of P_r, indicating that no photoreaction occurs at these temperatures. However, when actinic pumping is performed at temperatures above 45 K, new SERDS peaks are observed, the most prominent of which is at 829 cm^{-1}. These new peaks are assigned to the appearance of the primary photoproduct of P_r. When 647 nm actinic pumping is performed at higher temperatures, the peaks become more intense due to generation of more photoproduct, the largest percentage of which is observed when actinic pumping is performed at 150 K. The observation that these peaks are produced at 45 K and not at 20 K is consistent with the idea that we are observing the appearance of the primary photoproduct of P_r and that there is a thermally dependent activation barrier. The increased intensity of the SERDS peaks of this photoproduct with increased irradiation temperature between 45 and 150 K, coupled with the observation that lumi-R is trapped at 150 K (Eilfeld & Rudiger, 1985), show that the primary photoproduct of P_r is lumi-R. The intensity of the 829 cm^{-1} peak of lumi-R is plotted versus irradiation temperature in Figure 3. The appearance of lumi-R is fit with a single exponential function and the Arrhenius plot gives an apparent activation energy of 266 J/mol. The lumi-R intermediate could be completely converted back to P_r at 150 K with 716 nm illumination from a Ti:sapphire laser, indicating the reaction is fully photoreversible (data not shown). All subsequent experiments on the lumi-R intermediate were performed using 647 nm illumination at 150 K to generate this species.

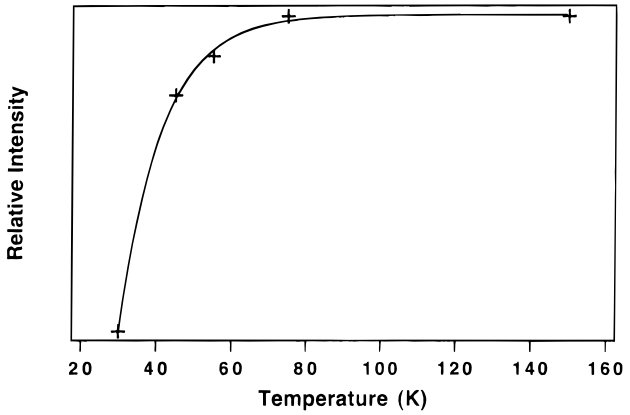

FIGURE 3: Intensity of the 829 cm^{-1} lumi-R peak as a function of irradiation temperature. The steady-state ratio of lumi-R produced as a function of temperature appears to follow a single exponential rise. The intensity of the 829 cm^{-1} lumi-R peak was measured relative to the 978 cm^{-1} peak of P_r.

Resonance Raman Spectrum of Lumi-R. Our method for obtaining the complete resonance Raman spectrum of lumi-R is illustrated in Figure 4. SERDS spectra of pure P_r (spectrum A) and a steady-state mixture of P_r and lumi-R (spectrum B) were acquired. The intensities of the lines in the P_r SERDS spectrum were scaled by a factor of 0.5 and then subtracted from the spectrum of the steady-state mixture of P_r and lumi-R. The choice of subtraction parameter was empirically determined on the basis of the removal of the P_r band at 805 cm^{-1}. The optimum subtraction parameter for the 805 cm^{-1} band also removed other prominent P_r lines at 1244, 1297, 1326, 1378, 1477, 1627, and 1642 cm^{-1}. The remaining lines in the SERDS spectrum due to scattering from lumi-R (spectrum C) were then integrated following standard procedures (Shreve et al., 1992), giving the Raman spectrum shown in (E). To provide initial information on vibrational assignments of the lumi-R spectrum, analogous spectra of lumi-R were obtained in a D_2O buffer (Figure 5). The parameters used for subtraction were equivalent to those of the H_2O spectra and removed P_r lines at 799, 1424, 1618, and 1634 cm^{-1}. The SERDS spectrum of lumi-R in D_2O buffer was then integrated, giving the Raman spectrum shown in Figure 5E. Additionally, the SERDS spectra of P_r and P_{fr} in H_2O and D_2O buffers were acquired, integrated, and plotted in Figures 6 and 7. These spectra are in excellent agreement with previously published spectra (Fodor et al., 1990).

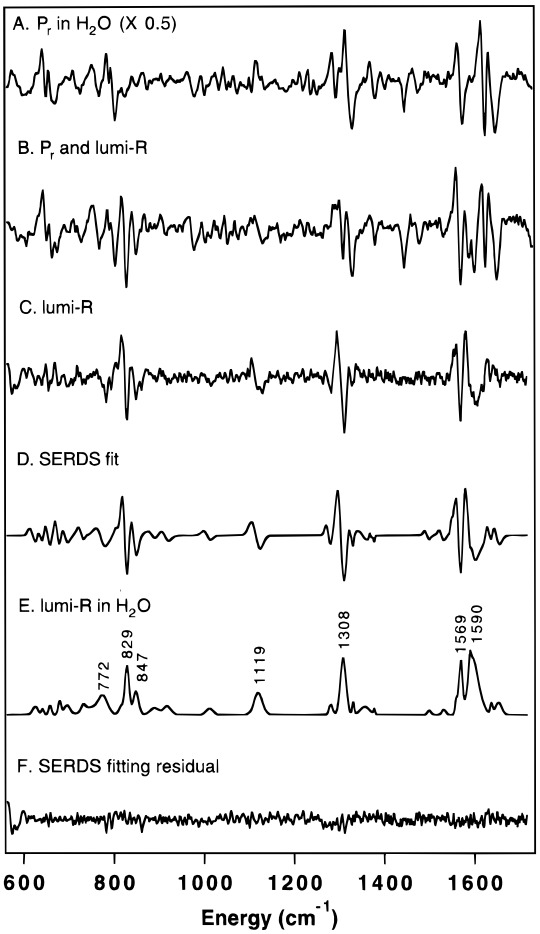

FIGURE 4: SERDS spectra of P_r (A), the steady-state mixture of P_r and lumi-R produced by irradiation with 647 nm light at 150 K (B), and the lumi-R SERDS spectrum in H_2O generated by subtracting the P_r spectrum from the steady-state mixture spectrum using a subtraction factor of 0.5 (C). The SERDS spectrum of lumi-R was fit to a difference of Gaussian peaks (D), and the corresponding Raman spectrum was generated by integration (E). The SERDS fitting residual illustrates the quality of the fit (F). The excitation wavelength was 750 nm. Data were recorded at 150 K.

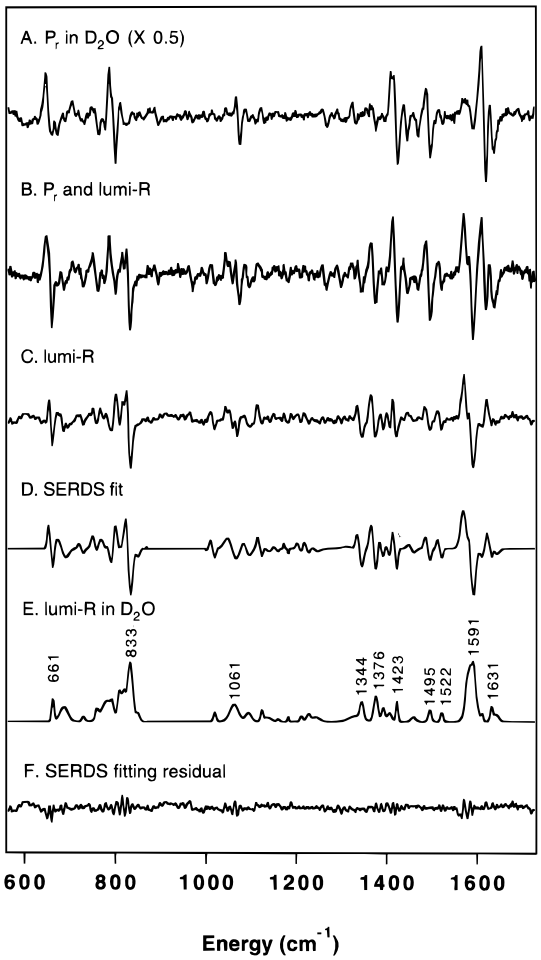

FIGURE 5: SERDS spectra of P_r (A), the steady-state mixture of P_r and lumi-R, produced by irradiation with 647 nm light at 150 K (B), and the lumi-R SERDS spectrum in D_2O generated by subtracting the P_r spectrum from the steady-state mixture spectrum using a subtraction factor of 0.5 (C). The SERDS spectrum of lumi-R was fit to a difference of Gaussian peaks (D), and the corresponding Raman spectrum was generated by integration (E). The SERDS fitting residual illustrates the quality of the fit (F). The excitation wavelength was 750 nm. Data were recorded at 150 K.

Comparison of the Raman spectra of P_r, lumi-R, and P_{fr} in Figure 6 illustrates that there are similarities as well as significant differences in their vibrational structure. The bands in the C═C and C═N stretching regions in the P_r spectrum at 1642, 1627, and 1576 cm^{-1} are replaced by bands at 1651, 1636, 1590, and 1569 cm^{-1} in the lumi-R spectrum. It appears that the intense bands at 1642 and 1627 cm^{-1} in P_r have shifted down to ∼1590 cm^{-1} in lumi-R. Additionally, the intense 1326 cm^{-1} P_r band in the N−H rocking region shifts to 1308 cm^{-1} in lumi-R. The strong 805 cm^{-1} band in the C−H wagging region of P_r is replaced with a band at 829 cm^{-1} and an additional band at 847 cm^{-1}. Comparing the lumi-R and P_{fr} spectra in Figure 6 we note that the bands at 1651, 1636, 1590, and 1569 cm^{-1} in the lumi-R spectrum are replaced by bands at 1619, 1598, and 1552 cm^{-1} in the P_{fr} spectrum. The 1569 cm^{-1} band has dropped in frequency and intensity to 1552 cm^{-1} and the intense C═C band at 1590 cm^{-1} has shifted up to 1598 cm^{-1}. The band at 1308 cm^{-1} in the N−H rocking region of lumi-R is replaced by a band centered at 1301 cm^{-1} in P_{fr}. The lumi-R C−H wagging modes at 829 and 847 cm^{-1} are replaced by one extremely intense band at 814 cm^{-1} and a minor band at 845 cm^{-1} in P_{fr}. The resonance Raman spectrum of P_r also contains several bands in the region of 900−1300 cm^{-1} that are probably due to C−C stretching and C−H and CH_3 rocking modes which have been observed by others (Fodor et al., 1990; Fodor et al., 1988; Matysik et al., 1995). In this region, the lumi-R spectrum has peaks at 1119 and 1011 cm^{-1}, and the P_{fr} spectrum has peaks at 1158, 1136, 1050, and 1004 cm^{-1}.

Figure 7 presents a comparison of the resonance Raman spectra of P_r, lumi-R, and P_{fr} in D_2O. In D_2O, we expect the pyrrole N−H protons to be exchanged for deuterium so N−H modes will shift down in frequency along with other coupled modes exhibiting C═NH stretching character, thereby allowing qualitative assignment. In the C═C and C═NH stretching regions we observe frequency changes upon N-deuteration for P_r, lumi-R, and P_{fr}. The peaks at 1642, 1627, and 1576 cm^{-1} for P_r in H_2O are replaced by peaks at 1634, 1618, and 1590 cm^{-1} in D_2O. The peaks at 1642 and 1627 cm^{-1} exhibit 8 and 9 cm^{-1} downshifts, respectively, suggesting that these are C═C stretching modes. For P_r, a peak occurs at 1590 cm^{-1} upon N-deuteration. This peak has probably shifted down from ∼1642 cm^{-1} after isotope exchange as suggested by the loss of intensity in

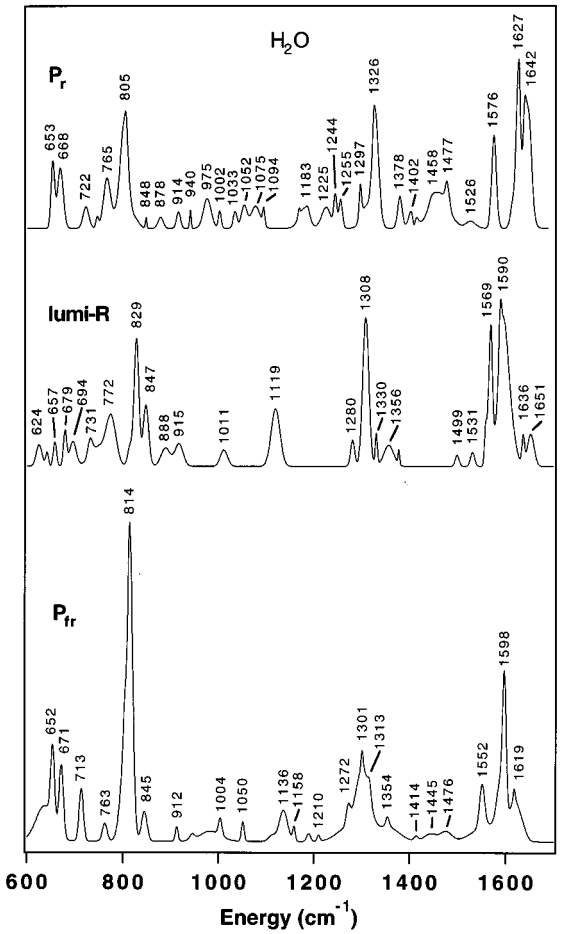

FIGURE 6: Raman spectra of P_r, lumi-R, and P_{fr} in H_2O. The Raman spectrum of P_r was generated from the SERDS spectrum of P_r in Figure 4A. The Raman spectrum of P_{fr} was obtained from a flowing solution of phytochrome at room temperature using a 647 nm pump beam, a 750 nm probe beam and the SERDS technique.

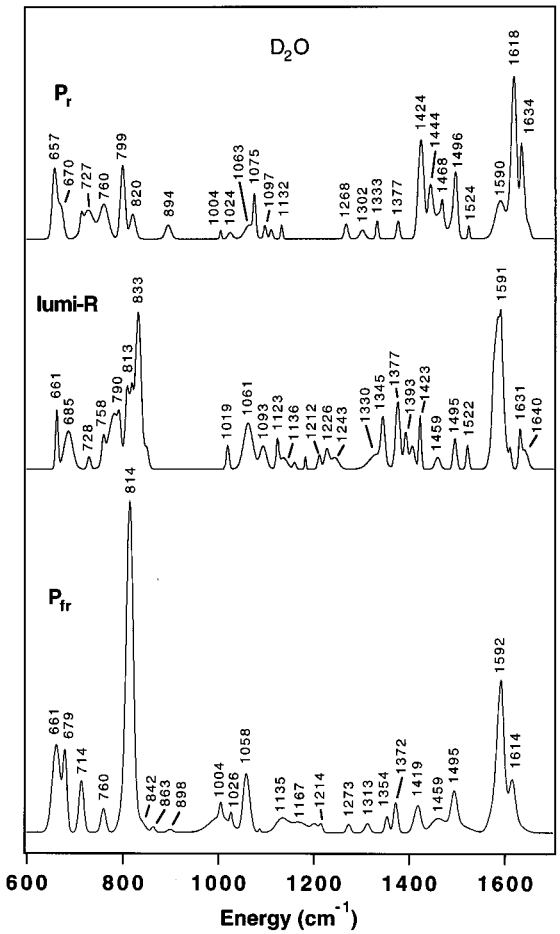

FIGURE 7: Raman spectra of P_r, lumi-R, and P_{fr} in D_2O. The Raman spectrum of P_r was generated from the SERDS spectrum of P_r in Figure 5A. The Raman spectrum of P_{fr} was obtained from a flowing solution of phytochrome at room temperature using a 647 nm pump beam, a 750 nm probe beam, and the SERDS technique.

this region. This downshift indicates that this mode may be a C═O stretch that is coupled to an N−H rock. The peak at 1576 cm^{-1} downshifts to 1496 cm^{-1} (Fodor et al., 1990), indicating that it has significant C═NH stretching character and that it is strongly coupled to an N−H rock. Three major peaks occur in the C═C stretching region of the lumi-R D_2O spectrum at 1640, 1631, and 1591 cm^{-1}. The 1651 cm^{-1} peak (H_2O) shifts to 1640 cm^{-1} upon N-deuteration, suggesting that this band is a C═O stretching mode coupled to an N−H rock. Furthermore, the 1590 cm^{-1} peak experiences almost no shift upon deuterium exchange, indicating no coupling of this C═C stretch to N−H rocking. However, the 1569 cm^{-1} peak shifts much more in D_2O (perhaps to 1495 or 1522 cm^{-1}), indicating that it is strongly coupled with the N−H rock coordinates. The most reasonable assignment of the 1569 cm^{-1} peak is to a delocalized double bond stretching mode involving the C═NH stretch. For P_{fr}, we observe peaks at 1619 and 1598 cm^{-1} in H_2O that experience small shifts to 1614 and 1592 cm^{-1} upon N-deuteration as expected for C═C stretching modes. But, the peak at 1552 cm^{-1} in H_2O shifts down to 1495 cm^{-1} in D_2O indicating that this peak is a C═NH stretching mode strongly coupled to an N−H rock.

We expect to observe C−C stretching, C−H rocking, and N−H rocking modes in the 1200−1400 cm^{-1} region of the Raman spectra of phytochrome. For P_r, the band at 1326 cm^{-1} has been assigned as an N−H rock through isotopic substitution, comparison to model compounds and normal mode analysis (Fodor et al., 1988, 1990). The observation that the most intense band in this region of our D_2O spectra is at 1075 cm^{-1} suggests that it is the N−D rock, consistent with this N−H rock assignment. The bands at 1225, 1244, and 1255 cm^{-1} are most likely C−H rocking modes. For lumi-R, the bands centered around 1308 cm^{-1} in H_2O (Figure 6) have shifted down to 1061 cm^{-1} in D_2O (Figure 7). We assign this to an N−H rocking mode which is expected to shift down upon N-deuteration by roughly 300 cm^{-1} (Curry et al., 1985). For P_{fr}, a strong band is found centered at 1301 cm^{-1} and downshifts to 1058 cm^{-1} in D_2O, consistent with the assignment of these bands as N−H rocking modes (Fodor et al., 1990). The assignments of N−H rocking modes is further corroborated by QCFF-π calculations we have performed involving N-deuterated model compound analogs which predict that N−D rocking modes occur at ∼1050 cm^{-1}.

The lower frequency bands of phytochrome observed between 800 and 900 cm^{-1} can be due to hydrogen out-of-plane modes. In P_r, the peak at 805 cm^{-1} is a likely candidate for this type of vibration (Fodor et al., 1990). Upon deuterium exchange, we observe two peaks at 799 and 820 cm^{-1}. The small frequency shifts indicate that they are C−H wagging modes which are slightly coupled to N−H vibrations. Two peaks occur in the C−H wagging region for lumi-R at 847 and 829 cm^{-1}. On the basis of the intensities

in the H_2O and D_2O spectra, the 829 cm^{-1} peak shifts up to 833 cm^{-1} upon N-deuteration and the 847 cm^{-1} peak downshifts to 813 cm^{-1}. The upshift of the 829 cm^{-1} band would indicate that this is a C−H out-of-plane wagging mode whose coupling with N−H modes is altered upon N-deuteration. The downshift of the 847 cm^{-1} band would suggest that this is a C−H out-of-plane mode that is strongly coupled to an N−H out-of-plane wag. For P_{fr}, one dominant band is observed at 814 cm^{-1} in both H_2O and D_2O solvents. Additionally, P_{fr} exhibits a minor band at 845 cm^{-1} in H_2O that may persist as the 842 cm^{-1} shoulder in D_2O. The insensitivity of these bands to N-deuteration indicates that they are good candidates for C−H out-of-plane vibrations and are not N−H wagging vibrations.

Vibrational Calculations. The model compound used here differs from that used in earlier calculations (Fodor et al., 1990) in that we have adopted the C_{10}-*E,anti* geometry. This model is based on previous arguments (Fodor et al., 1990) and experimental evidence which suggests the chromophore exhibits this extended structure (Li et al., 1995; Tokutomi et al., 1992). The C_{10}-*E* geometry differs from the C_{10}-*Z* geometry of phytochromopeptides determined using ^{1}H NMR spectroscopy (Rudiger et al., 1983). However, the chromopeptides exhibiting the C_{10}-*E* geometry are expected to undergo rapid prototropic shifts and tautomerization at room temperature, ultimately resulting in a thermal C_{10}-*E* → C_{10}-*Z* isomerization to the lowest energy structure (Falk, 1989). Therefore, the C_{10}-*E* chromophore geometry *in situ* is not inconsistent with the conclusions drawn for the chromopeptides (Rudiger et al., 1983).

The geometry about the C_5 exocyclic carbon for the model compounds used in our vibrational calculations is the extended C_4═C_5, C_5−C_6, *Z,anti* structure as found for the chromophore structure in C-phycocyanin (Schirmer et al., 1987). This contrasts with the suggestion that this geometry is *Z,syn* on the basis of comparison of the oscillator strength ratios of the visible absorption bands with results of SCF-MO calculations (Song et al., 1979). However, the assignment and interpretation of the electronic absorption bands are open to interpretation, and the model compounds used in these calculations were not fully protonated (Song & Chae, 1979). In any event, our vibrational calculations are insensitive to the bonding geometry about the C_5 exocyclic carbon because the π-conjugation does not extend into the A ring of the chromophore.

Normal mode calculations with a deprotonated chromophore give rise to vibrational frequencies and intensities similar to those involving the fully protonated chromophore, and therefore, an independent unambiguous determination of the protonation state is essential. We have observed bands in the P_r, lumi-R, and P_{fr} spectra that can be assigned as C═N stretching vibrations on the basis of apparent frequency shifts due to N-deuteration. At the present level of understanding of the phytochrome vibrational spectra, this suggests that the pyrrolenic and lactam nitrogens of the phytochrome chromophore are protonated irregardless of whether the C═N bond is in the B, C, or D rings and that the chromophore is cationic in all three species. If these mode assignments are correct, then the most consistent model with respect to our observed spectra involves a chromophore that is fully protonated in P_r, lumi-R, and P_{fr}.

The calculated vibrational frequencies and intensities of selected modes for the four cationic isomers are displayed in Figure 8, and the energy-minimized structures used in the calculations are displayed in Figure 9. For the phytochrome chromophore, normal mode analysis using QCFF-π predicts significant differences in frequency and intensity for C═C stretching, N−H rocking, and C−H wagging modes in response to geometry changes about the C_{15} methine bridge. We now describe these differences.

Table 1: Minimized Geometry of the Phytochrome Chromophore[a]

	C_{15}-*Z,syn*	C_{15}-*Z,anti*	C_{15}-*E,syn*	C_{15}-*E,anti*
C_4═C_5	179.2	179.2	179.1	179.2
C_5−C_6	−49.4	−49.4	−49.3	−49.4
C_9−C_{10}	11.1	12.2	10.9	11.4
C_{10}═C_{11}	51.3	48.9	51.3	50.9
C_{14}−C_{15}	173.7	147.4	−26.5	−139.5
C_{15}═C_{16}	177.9	176.2	−15.4	13.8

[a] Torsional angles about the indicated bonds in degrees.

The ethylenic stretching region shows sensitivity to changes in structure. Comparing the C_{14}−C_{15} *syn* to C_{14}−C_{15} *anti* structure, a 10−20 cm^{-1} decrease in frequency of the 1570 cm^{-1} (*Z,syn*) and 1574 cm^{-1} (*E,syn*) ethylenic modes as well as a splitting is predicted. This mode also exhibits a large degree of N−H and C−H rocking character, suggesting that these rocking modes are mixed with the ethylenic stretches. This mode may provide a marker band for C_{14}−C_{15} conformation because it shifts down in frequency for both C_{14}−C_{15} *anti* structures.

The N−H rocking and C−H rocking modes are strongly coupled, and their mode frequencies shift when the geometry of the C_{15} methine bridge is altered. The first obvious trend is the frequency downshift of modes at 1321 and 1301 cm^{-1} in the C_{15}-*Z,syn* structure to the range of 1281−1285 cm^{-1} for the other three isomers. These frequencies are correlated by their similarity of vibrational motion; they exhibit strong N−H rocking character of the B and C ring nitrogens as well as contributions from C_{10}−H and C_{15}−H rocking and C_{14}−C_{15} stretching motions. The other noticeable change elucidated by the QCFF-π calculation is the large intensity of the 1264 and 1257 cm^{-1} A and B ring N−H and the C_{10}−H and C_{15}−H rocking modes for the C_{15}-*Z* configurations as compared to the C_{15}−*E* configurations.

QCFF-π predicts small frequency shifts and large intensity changes for the C−H wagging modes when the geometry about the C_{15} methine bridge is changed. The calculations also indicate that the C_5−H, C_{10}−H, and C_{15}−H wagging modes are strongly coupled. The most significant predicted change is the increased C−H wagging intensity for the *E,anti* geometry compared to the other isomers. This is due to the large angle between the C and D rings (Table 1 and Figure 9) which allows the C−H wagging motions to effectively mix with ethylenic stretching modes and thereby gain intensity. The minimized geometry for the *Z,syn* isomer has a relative angle of 6° between the C and D rings, and the smallest C−H wagging intensity is predicted. For the *Z,anti* and *E,syn* geometries this angle is roughly 30° and 25°, respectively, and these structures therefore exhibit moderate C−H wagging intensities.

These observations suggest that the degree of planarization of adjacent pyrrolenic/lactam rings in the chromophore determines how effectively each type of C−H vibrational motion mixes with ethylenic stretches and controls their resonance Raman intensity. As the rings become planar, the C−H rocking motions effectively mix with the ethylenic

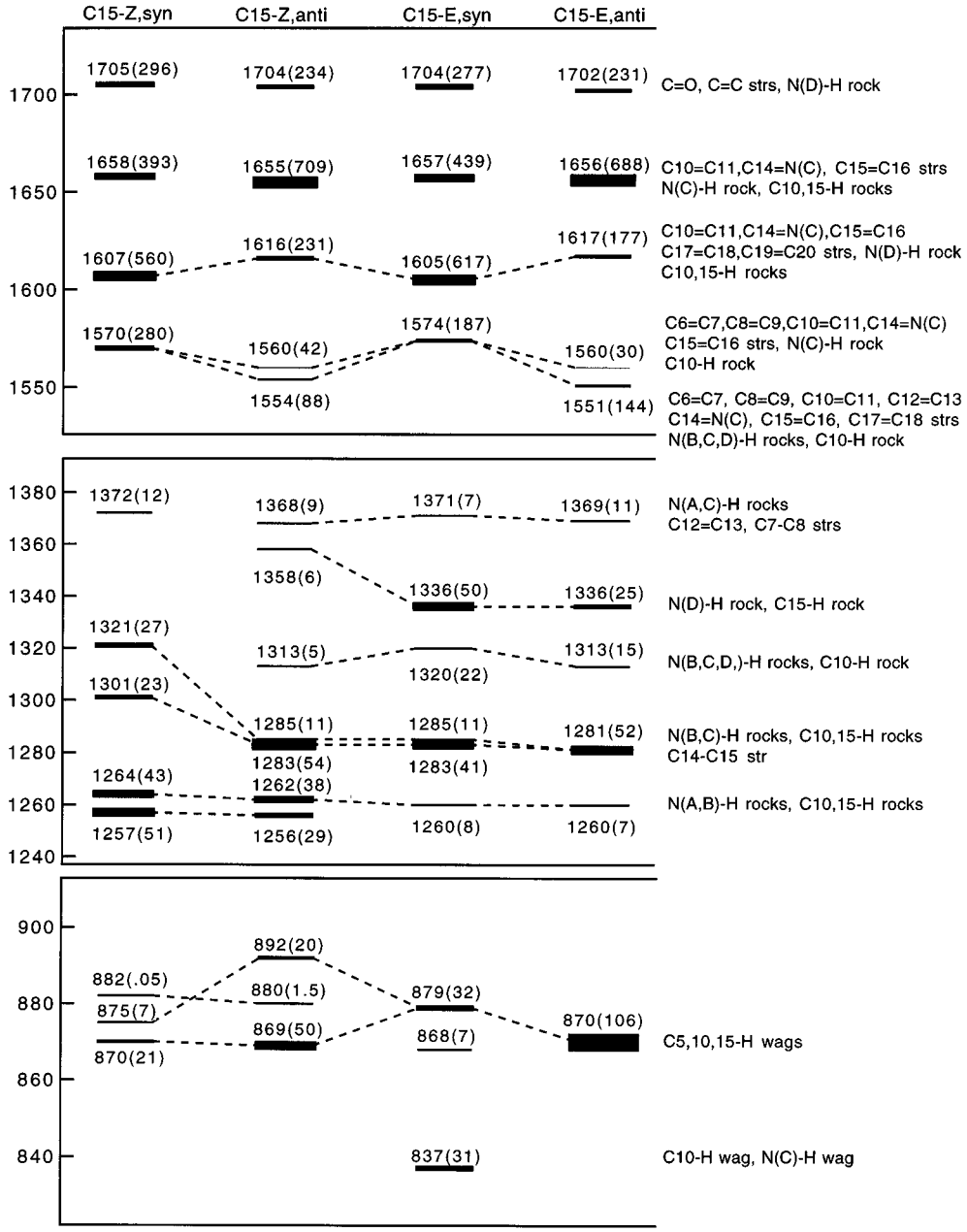

FIGURE 8: Correlation diagram of the calculated vibrational frequencies for the four structural isomers of the phytochrome chromophore model compound displayed in Figure 9. Relative Raman intensities of each mode are qualitatively represented by the line thickness and are quantitatively given in parentheses.

stretches and gain intensity whereas the C−H wagging motions lose intensity. Conversely, if the rings are nonplanar, the C−H wagging motions mix with the ethylenic stretches and gain intensity whereas the C−H rocking motions lose intensity. Therefore, relative intensities of the C−H rocking and wagging motions provide marker bands for the degree of planarization of the rings of the tetrapyrrole chromophore.

DISCUSSION

Chromophore Structure and Reaction Mechanism in the Photocycle. We have obtained resonance Raman spectra of P_r and its primary photoproduct, lumi-R, with the goal of examining the nature of the primary photochemical event. The resonance Raman spectra of phytochrome presented here provide valuable *in situ* information about the structural changes of the chromophore that must occur during the P_r → lumi-R photoconversion. This primary step could involve a concerted C_{15}-*Z,syn* to C_{15}-*E,anti* photoisomerization or a C_{15}═C_{16} photoisomerization alone which is later followed by a conformational rotation about the C_{14}−C_{15} bond. Changes about the C_{15} methine bridge are of particular interest because they control the location of the D ring and thereby the spatial position of the adjoining N−H and C═O functional groups. The frequencies and intensities of the vibrational bands of P_r, lumi-R, and P_{fr} differ significantly, indicating that the chromophore geometry is different in all three species. We now present evidence as to what these structures are.

The observed spectral changes for the P_r → lumi-R photoconversion are most consistent with an isomerization of the C_{15}═C_{16} bond from C_{15}-*Z,syn* in P_r to C_{15}-*E,syn* in lumi-R. This conclusion is based on the following observations: First, the normal mode calculations predict that a change from a C_{15}-*Z,syn* geometry to any other C_{15} isomer

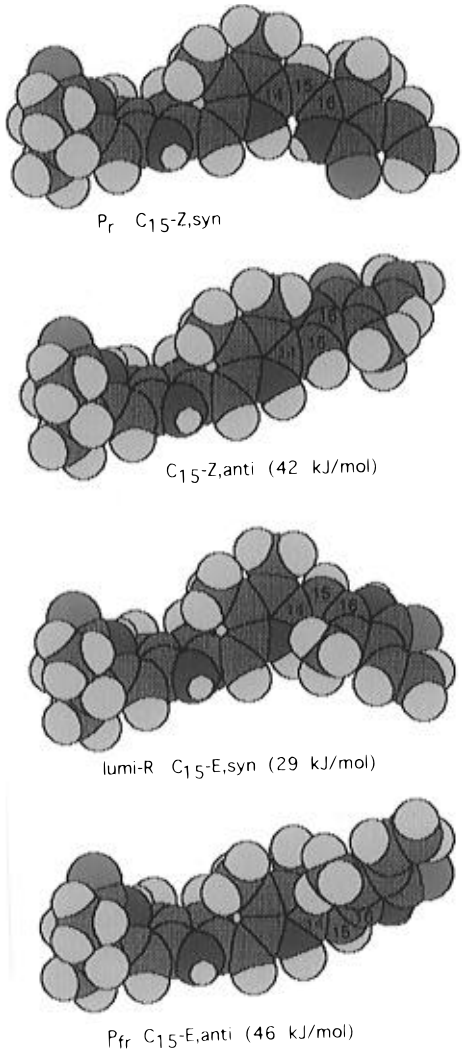

FIGURE 9: Four structural isomers of the model compound used in the normal mode analysis of phytochrome. Displayed are the space-filling models for the C_5-*Z,anti*, C_{10}-*E,anti*, C_{15}-*Z,syn* geometry and its four structural isomers generated by rotating about either the $C_{14}-C_{15}$ or $C_{15}=C_{16}$ bonds. Conformational and configurational angles about the methine bridging bonds are listed in Table 1. Energies of each minimized structure relative to the P_r structure are also indicated.

will result in a frequency lowering of the N−H rocking modes. The bands at 1326 cm^{-1} in P_r and 1308 cm^{-1} in lumi-R can reliably be assigned as N−H rocking modes on the basis of their frequency shifts upon N-deuteration. This indicates that the P_r chromophore has the C_{15}-*Z,syn* geometry and that upon photolysis a geometric change occurs at the C_{15} methine bridge to form one of the other possible isomers. Second, our calculations predict that the C=N stretching vibration is a diagnostic marker for the $C_{14}-C_{15}$ single bond conformation since this band is predicted to downshift 10−20 cm^{-1} when a *syn* → *anti* conformational change occurs. On the basis of shifts that occur upon N-deuteration, we have identified C=N stretching vibrations at 1576 and 1569 cm^{-1} in P_r and lumi-R, respectively. The lack of frequency drop of this band in the lumi-R spectrum as compared to the P_r spectrum strongly suggests that the $C_{14}-C_{15}$ *syn* conformation is maintained during the phototransition.

Our resonance Raman spectra further indicate that the lumi-R → P_{fr} interconversion involves conformational isomerization about the $C_{14}-C_{15}$ bond to give the *anti* isomer. This proposal is supported by the following evidence. Our normal mode analysis predicts a 2−5 cm^{-1} drop in N−H rocking frequency when a C_{15}-*E,syn* → C_{15}-*E,anti* geometry change occurs. The N−H rocking band of lumi-R at 1308 cm^{-1} decreases in frequency upon the lumi-R → P_{fr} interconversion to 1301 cm^{-1}. Also, the 1569 cm^{-1} band of lumi-R shifts to 1552 cm^{-1} in P_{fr}. This band exhibits strong C=N stretching character as shown by its frequency shift upon N-deuteration. The 17 cm^{-1} downshift of this band in the lumi-R → P_{fr} interconversion, a result predicted by our normal mode analysis, also supports a *syn* → *anti* conformational change. In addition, our calculations show that the C_{15}-*E,anti* geometry exhibits C−H wagging intensity 3−4-fold greater than that of the C_{15}-*Z,syn* or C_{15}-*E,syn* geometries. We have assigned C−H wagging modes in lumi-R at 829 and 847 cm^{-1} and in P_{fr} at 814 cm^{-1}. In general, normal mode calculations for the structures depicted in Figure 9 indicate that elevated intensity of the C−H wagging modes and decreased intensity of C−H rocking modes occur for geometries having increased distortion about the C_{15} methine bridge. The isomer which exhibits the most distortion is the C_{15}-*E,anti* geometry caused by the steric interaction of the C and D ring methyl groups. The 3-fold increase of the 814 cm^{-1} band in P_{fr} as compared to the 829 cm^{-1} band in lumi-R suggests the C and D rings are nonplanar in P_{fr}, supporting the hypothesis that the chromophore geometry in P_{fr} is C_{15}-*E,anti*.

The C_{15}-*Z,anti* chromophore geometry is predicted to have two strong C−H wagging modes at 869 and 892 cm^{-1} and is also a candidate for the chromophore structure of lumi-R, *prima facie*. However, the lack of a large frequency downshift of the C=N stretching marker band upon photoconversion to lumi-R and NMR studies on phytochromopeptides (Rudiger et al., 1983) indicate that a *Z* → *E* isomerization occurs in the P_r → P_{fr} interconversion. In addition, saturation of the $C_{15}=C_{16}$ bond of the phytochrome chromophore eliminates the photochemistry (Li & Lagarias, 1992; Li et al., 1995). On the basis of these arguments, we conclude that the chromophore geometry in lumi-R is C_{15}-*E,syn*.

It has been discussed that the primary photochemical step in the Pr → P_{fr} phototransformation could be a sequential $C_{15}=C_{16}$ *Z* → *E* photoisomerization followed by a nonphotochemical $C_{14}-C_{15}$ conformational change or simultaneous, photochemical $C_{14}-C_{15}$, $C_{15}=C_{16}$ bond rotations (Fodor et al., 1990; Rudiger, 1992). Photoisomerization of the $C_{15}=C_{16}$ bond to the *E* geometry forming lumi-R followed by subsequent $C_{14}-C_{15}$ conformational relaxation to the *anti* geometry forming P_{fr} is most consistent with the vibrational spectra presented here. Additional evidence supporting the sequential C=C and C−C bond rotations is provided by time-resolved absorption experiments performed by Kandori et al. (1992), who determined that the appearance time for lumi-R is 24 ps. This is roughly the time scale observed for the *cis*−*trans* isomerization of dipyrroles (Falk, 1989). If the primary photochemistry were a simultaneous rotation of adjacent single and double bonds, an event best described as tunneling, we would expect to observe photoproduct formation times for lumi-R that are significantly faster. Thus, the observation that lumi-R production does not occur on the femtosecond time scale supports our conclusion that the P_r → lumi-R photochemistry is best described by a $C_{15}=C_{16}$ double bond photoisomerization.

On the basis of vibrational spectra and normal mode analysis of biliverdin dimethyl ester (Smit et al., 1993), Matysik et al. (1995) suggested that the $P_r \rightarrow$ lumi-R transition may be interpreted as an isomerization of a double bond and conformational relaxation about two single bonds. They also conclude that the chromophore of phytochrome is fully protonated in the lumi-R intermediate. However, their Raman spectra of lumi-R may suffer from incomplete subtraction of the P_r spectral contribution resulting in potentially erroneous conclusions. We have found that changes of the bonding geometry about just the C_{15} exocyclic carbon provide a consistent model for interpreting our spectra.

We have determined an activation energy mol^{-1} barrier for the $P_r \rightarrow$ lumi-R photoconversion of 266 J mol^{-1} on the basis of the temperature-dependent appearance of the 829 cm^{-1} vibrational band of lumi-R. Previously, Eilfeld et al. (1986) determined the activation energy for this process to be ~3.6 kJ mol^{-1} using low-temperature trapping and absorption experiments between 119 and 155 K. This apparent discrepancy may be in part rationalized by the fact that Arrhenius plots reported by these investigators exhibited nonlinearity best described by biexponential fits. In this regard, Sineshchekov et al. (1990) derived activation energies for the P_r photoconversion of 17−20 kJ mol^{-1} between 200 and 270 K ($P_r \rightarrow P_{fr}$) and 2.7−3.0 kJ mol^{-1} between 80 and 200 K ($P_r \rightarrow$ lumi-R) on the basis of photoinduced changes of P_r fluorescence. Our measured activation energy of the $P_r \rightarrow$ lumi-R photoconversion, which is significantly lower than the values reported by these investigators, may be due to the fact that our value was determined using data obtained in the 30−155 K temperature range.

Temperature dependence studies of the $P_r \rightarrow$ lumi-R photochemistry below 30 K have not been previously reported. At these temperatures conformational relaxation of an amino acid can be thermally prevented. If dynamic thermal fluctuations of residues in the protein binding pocket are required for photochemical activity, then this loss of photochemistry can be understood. We propose that D ring rotation which accompanies the C_{15}═C_{16} isomerization is blocked by an adjacent amino acid that has been conformationally frozen at low temperature. The observation of increased fluorescence intensity upon lowering the temperature (Sineshchekov et al., 1990; Song et al., 1975; our unpublished data) also suggests that the chromophore becomes locked into a more rigid molecular structure at low temperature. Elimination of the photochemistry is best represented by an altered excited-state potential energy surface below 30 K. This change results in the inaccessibility of the C_{15}═C_{16}, 90° excited-state geometry which prevents complete rotation about the C_{15}═C_{16} bond to form the C_{15}-*E* isomer. At temperatures above 30 K, the conformational change of an amino acid within the chromophore binding pocket of phytochrome is no longer thermally prevented, and the photoexcited chromophore can relax on the excited-state surface to give the C_{15}═C_{16}, 90° geometry. Decay to the ground state would give either the C_{15}-*E,syn* lumi-R photoproduct or the C_{15}-*Z,syn* P_r reactant since the photoreaction quantum yield is not 100% (Gensch et al., 1996; Lagarias et al., 1987; unpublished data). The change in orientation of the D ring in the lumi-R intermediate (C_{15}-*E,syn*) depicted in Figure 9 then initiates subsequent protein conformational changes.

After the primary photoconversion, lumi-R $\rightarrow P_{fr}$ interconversion involves a *syn* → *anti* conformational change about the C_{14}−C_{15} bond. The C_{14}−C_{15} *anti* conformation in P_{fr} results in nonplanar C and D ring moieties due to steric interaction of the C and D ring methyl groups of the chromophore. QCFF-π analysis predicts relative energies of 29 and 46 kJ mol^{-1} for the lumi-R (C_{15}-*E,syn*) and P_{fr} (C15-*E,anti*) chromophore structures, respectively (Figure 9). This forces us to ask why the chromophore is drawn to the distorted, high-energy structure in P_{fr} and how can this chromophore geometry be stablilized.

One way of stabilizing the high-energy chromophore structure in P_{fr} is through specific chromophore−protein interactions. Hydrogen bond formation between the protein and the N−H and/or C═O functional groups of the D ring of the chromophore could provide a stabilization mechanism. Ultimately, when considering the chromophore and apoprotein as a whole, the free energy of the P_{fr} molecule must be lower than the free energy of the lumi-R molecule. This is consistent with the following facts: lumi-R must be thermally trapped, P_{fr} is a thermostable species at room temperature, and the lumi-R $\rightarrow P_{fr}$ interconversion is a spontaneous process at room temperature. The idea of hydrogen bond formation may also help to explain the 30−100 nm bathochromic shift and increased oscillator strength of the visible absorption of phytochrome relative to C-phycocyanin trimers which lack significant D ring hydrogen bond contacts (Schirmer et al., 1987; Duerring et al., 1991). Lactim-containing model compounds also show correspondingly bathochromic spectra as compared to their lactam counterparts (McDonagh, 1979; Micura & Grubmayr, 1994), further supporting this idea.

Model for Chromophore Stabilization in the Phytochrome Photocycle. On the basis of the preceding discussion, we present in Figure 10 a model depicting the chromophore geometries in the photocycle of phytochrome along with postulated protein hydrogen-bonding contacts that provide chromophore stabilization. The D ring N−H and C═O groups of the P_r chromophore are assumed to be hydrogen bonded to acceptor A_1 and donor D_1 amino acids and/or amide constituents of the protein backbone resulting in thermostability of this species.[2] Photochemical conversion to the C_{15}-*E,syn* lumi-R species breaks these chromophore−protein interactions. The lumi-R chromophore geometry is now in an unfavorable bonding environment due to interaction of the D ring vinyl and methyl hydrophobic groups with protein hydrophilic groups, and therefore the free energy of this species is high. A conformational change of the C_{14}−C_{15} bond then occurs which is driven by the high energy of the lumi-R species. The newly formed C_{15}═C_{16}, C_{14}−C_{15}, *E,anti* chromophore structure is then stabilized by contacts between the N−H and C═O groups of the D ring and two new hydrogen bond acceptor A_2 and donor D_2 groups. The 46 kJ mol^{-1} energy increase of the highly distorted P_{fr} chromophore is thereby compensated by hydrogen bond

[2] Although we present the idea of hydrogen-bonding contacts between the chromophore and protein in P_r as a stabilizing mechanism, the fact that the C_{15}═C_{16}, C_{14}−C_{15}, *Z,syn* geometry is the lowest energy isomer may indicate that these contacts are not critical in stabilizing the chromophore in this species.

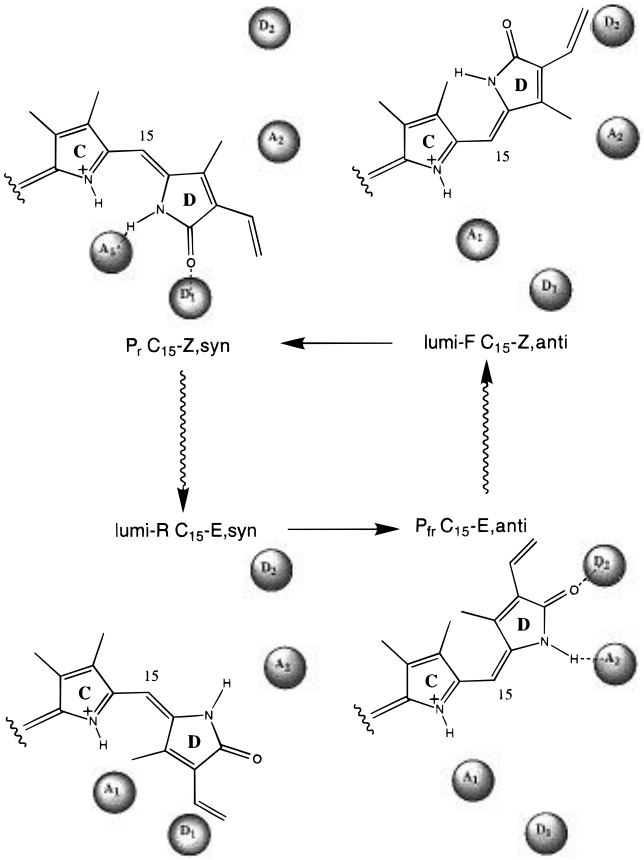

FIGURE 10: Model of chromophore structure and the molecular mechanism of the photocycle of phytochrome. Shown are the chromophore geometries in P_r, lumi-R, and P_{fr} along with the predicted geometry of lumi-F and postulated hydrogen bond accepting and donating amino acid side chains or amide backbone constituents.

formation which is expected to contribute ~20 kJ mol^{-1} stabilization energy per hydrogen bond. The indicated changes in hydrogen-bonding contacts that occur in the P_r → lumi-R photoconversion are supported by the recent findings of a molecular expansion of 7 mL mol^{-1} (11 Å^3/molecule) that accompanies the photoconversion using laser-induced optoacoustic spectroscopy (Gensch et al., 1996).

This model has important implications concerning the protein conformational changes that accompany the P_r → P_{fr} interconversion, the thermostability of P_{fr}, and the mechanism of the P_{fr} → P_r interconversion. The release of the A_1 and D_1 constituents of the protein upon P_r → P_{fr} photoconversion could allow this region of the protein to adopt a new conformation. Furthermore, the formation of new hydrogen-bonding contacts between the P_{fr} chromophore and A_2 and D_2 would anchor a different region of the protein. This anchor and release mechanism could initiate the protein structural changes required for altered phytochrome signaling. Additionally, this model indicates that dark reversion of P_{fr} → P_r through tautomerization and/or prototropic shifts is prevented by stabilizing hydrogen-bonding contacts. Without these contacts dark reversion is not prevented as indicated by ^{1}H NMR studies of the P_{fr} phytochromopeptide (Rudiger et al., 1983). We may also use this model to develop a hypothesis about the reverse P_{fr} → P_r interconversion. Presumably, the P_{fr} chromophore undergoes photochemical isomerization of the C_{15}═C_{16} bond to produce the C_{15}-*Z,anti* structure which would be the chromophore geometry in the primary photoproduct of P_{fr}, lumi-F. This breaks the stabilizing hydrogen bonds to A_2 and D_2. A C_{14}−C_{15} *anti to syn* conformational isomerization is then driven by the unfavorable fit of the *anti* conformer and the re-formation of hydrogen bonds with A_1 and D_1. This results in the hydrogen-bonded C_{15}═C_{16}, C_{14}−C_{15}, *Z,-syn* geometry of the thermostable P_r chromophore. Structural studies on the chromophore in lumi-F are called for to test this hypothesis. In this regard, Matysik et al. (1995) have obtained Fourier transform Raman spectra of lumi-F in H_2O and D_2O using low-temperature trapping, showing that it should be possible to obtain data to test this hypothesis.

We envision further experiments to test our model for the chromophore and protein changes that accompany the phytochrome photocycle. Since expression, assembly, and purification of recombinant phytochrome have been accomplished (Murphy & Lagarias, 1996), this model may be critically examined using novel chromophore analog−apophytochrome adducts and site-directed mutagenesis. Additionally, synthesis of a $C_{5,10,15}$−deuterium chromophore analog has been accomplished by Lugtenberg and co-workers (personal communication), and construction of this phytochrome adduct will allow mode assignments to further refine our model. Furthermore, site-directed mutagenesis can be used to reveal amino acids involved in hydrogen-bonding contact with the chromophore. Studies of protein structure of phytochrome via ultraviolet resonance Raman spectroscopy indicate that significant changes occur in a few tryptophan residues on the basis of comparison of tryptophan Raman bands of P_r and P_{fr} (Mizutani et al., 1993; Toyama et al., 1993). Mizutani et al. (1993) were able to assign these changes to Trp^{365} and Trp^{567} on the basis of studies of a series of truncated Pea phytochromes. These residues are therefore implicated as likely candidates for hydrogen bond donors in our model.

CONCLUSION

Raman structural analysis of chromophore structure in phytochrome allows us to elucidate the molecular events in the phytochrome photocycle. The chromophore structure of the P_r form of phytochrome is C_{15}-*Z*. The primary photochemical event is a *Z* → *E* isomerization giving the C_{15}-*E,syn* structure in lumi-R. Subsequent interconversion to P_{fr} involves a conformational isomerization of the C_{14}−C_{15} bond to form the C_{15}-*E,anti* chromophore structure. The formation of the high-energy C_{15}-*E,anti* chromophore in P_{fr} is proposed to be stabilized by hydrogen-bonding interactions with the protein environment. This suggests that an anchor and release mechanism involving chromophore−protein hydrogen-bonding contacts might initiate subsequent protein structural changes that lead to altered biological signaling.

REFERENCES

Bjorling, S. C., Zhang, C.-F., Farrens, D. L., Song, P.-S., & Kliger, D. S. (1992) *J. Am. Chem. Soc. 114,* 4581−4588.

Bowler, C., Yamagata, H., Neuhaus, G., & Chua, N.-H. (1994) *Genes Dev. 8,* 2188−2202.

Brock, H., Ruzsicska, B. P., Arai, T., Schlamann, W., Holzwarth, A. R., Braslavsky, S., & Schaffner, K. (1987) *Biochemistry 26,* 1412−1417.

Chen, E., Lapko, V. N., Lewis, J. W., Song, P.-S., & Kliger, D. S. (1996) *Biochemistry 35,* 843−850.

Cherepy, N. J., Shreve, A. P., Moore, L. J., Boxer, S. G., & Mathies, R. A. (1994) *J. Phys. Chem. 98,* 6023−6029.

Cherepy, N. J., Holzwarth, A. R., & Mathies, R. A. (1995) *Biochemistry 34,* 5288−5293.
Curry, B., Palings, I., Broek, A. D., Pardoen, J. A., Lugtenburg, J., & Mathies, R. (1985) *Advances in Infrared and Raman Spectroscopy* (Clark, J. H., & Hester, R. E., Eds.) pp 115−178, Wiley, Heyden.
Duerring, M., Schmidt, G. B., & Huber, R. (1991) *J. Mol. Biol. 217,* 577−592.
Eilfeld, P., & Rudiger, W. (1985) *Z. Naturforsch. 40c,* 109−114.
Eilfeld, P., Eilfeld, P., & Rudiger, W. (1986) *Photochem. Photobiol. 44,* 761−769.
Elich, T. D., & Chory, J. (1994) *Plant Mol. Biol. 26,* 1315−1327.
Falk, H. (1989) *The Chemistry of Linear Oligopyrroles and Bile Pigments,* Springer-Verlag, Wien and New York.
Farrens, D. L., Holt, R. E., Rospendowski, B. N., Song, P.-S., & Cotton, T. M. (1989) *J. Am. Chem. Soc. 111,* 9162−9169.
Fodor, S. P. A., Lagarias, J. C., & Mathies, R. A. (1988) *Photochem. Photobiol. 48,* 129−136.
Fodor, S. P., Lagarias, J. C., & Mathies, R. A. (1990) *Biochemistry 29,* 11141−11146.
Gensch, T., Churio, M. S., Braslavsky, S. E., & Schaffner, K. (1996) *Photochem. Photobiol. 63,* 719−725.
Grimm, R., & Rudiger, W. (1986) *Z. Naturforsch. 41c,* 988−992.
Hildebrandt, P., Hoffmann, A., Lindemann, P., Heiber, G., Braslavsky, S. E., Schaffner, K., & Schrader, B. (1992) *Biochemistry 31,* 7957−7962.
Holt, R. E., Farrens, D. L., Song, P.-S., & Cotton, T. M. (1989) *J. Am. Chem. Soc. 111,* 9156−9162.
Kandori, H., Yoshihara, K., & Tokutomi, S. (1992) *J. Am. Chem. Soc. 114,* 10958−10959.
Kendrick, R. E., & Kronenberg, G. H. M. (1994) *Photomorphogenesis in Plants,* Martinus Nijhoff, Dordrecht.
Kochendoerfer, G. G., Verdegem, P. J. E., van der Hoef, I., Lugtenburg, J., & Mathies R. A. (1996) *Biochemistry* (in press).
Lagarias, J. C., & Rapoport, H. (1980) *J. Am. Chem. Soc. 102,* 4821−4828.
Lagarias, J. L., Kelly, J. M., Cyr, K. L., & Smith, W. O. (1987) *Photochem. Photobiol. 46,* 5−13.
Li, L., & Lagarias, J. C. (1992) *J. Biol. Chem. 267,* 19204−19210.
Li, L., Murphy, J. T., & Lagarias, J. C. (1995) *Biochemistry 34,* 7923−7930.
Mathies, R., & Yu, N.-T. (1978) *J. Raman Spectrosc. 7,* 349−352.
Mathies, R. A., Oseroff, A. R., & Stryer, L. (1976) *Proc. Natl. Acad. Sci. U.S.A. 73,* 1−5.
Matysik, J., Hildebrandt, P., Schlamann, W., Braslavsky, S., & Schaffner, K. (1995) *Biochemistry 34,* 10497−10507.
McDonagh, A. F. (1979) *The Porphyrins* (Dolphin, D., Ed.) pp 293−491, Academic Press, New York.
Micura, R., & Grubmayr, K. (1994) *Bioorg. Med. Chem. Lett. 4,* 2517−2522.
Miller, F. A., & Harney, B. M. (1970) *Appl. Spectrosc. 24,* 291−292.
Mizutani, Y., Tokutomi, S., Aoyagi, K., Horitsu, K., & Kitagawa, T. (1991) *Biochemistry 30,* 10693−10700.
Mizutani, Y., Tokutomi, S., Kaminaka, S., & Kitagawa, T. (1993) *Biochemistry 32,* 6916−6922.
Mizutani, Y., Tokutomi, S., & Kitagawa, T. (1994) *Biochemistry 33,* 153−158.
Murphy, J. T., & Lagarias, J. C. (1996) *Photochem. Photobiol.* (submitted for publication).
Myers , A. B., & Mathies R. A. (1987) *Biological Applications of Raman Spectrometry* (Spiro, T. G., Ed.) Vol. 2, pp 1−58, John Wiley & Sons, Inc., New York.
Pratt, L. H. (1995) *Photochem. Photobiol. 61,* 10−21.
Quail, P. H., Boylan, M. T., Parks, B. M., Short, T. W., Xu, Y., & Wagner, D. (1995) *Science 268,* 675−680.
Rudiger, W. (1992) *Photochem. Photobiol. 56,* 803−809.
Rudiger, W., Thummler, F., Cmiel, E., & Schneider, S. (1983) *Proc. Natl. Acad. Sci. U.S.A. 80,* 6244−6248.
Schirmer, T., Bode, W., & Huber, R. (1987) *J. Mol. Biol. 196,* 677−695.
Shreve, A. P., Cherepy, N. J., Franzen, S., Boxer, S. G., & Mathies, R. A. (1991) *Proc. Natl. Acad. Sci. U.S.A. 88,* 11207−11211.
Shreve, A. P., Cherepy, N. J., & Mathies, R. A. (1992) *Appl. Spectrosc. 46,* 707−711.
Sineshchekov, V. A., Lapko, V. N., Sineshchekov, A. V., Kozhuku, G. V., & Udal'tsov, A. V. (1990) *J. Photochem. Photobiol., B. 5,* 219−229.
Smit, K., Matysik, J., Hildebrandt, P., & Mark, F. (1993) *J. Phys. Chem. 97,* 11887−11900.
Song, P.-S. (1988) *J. Photochem. Photobiol., B. 2,* 43−57.
Song, P.-S., & Chae, Q. (1979) *Photochem. Photobiol. 30,* 117−123.
Song, P.-S., Chae, Q., & Briggs, W. R. (1975) *Photochem. Photobiol. 22,* 75−76.
Song, P.-S., Chae, Q., & Gardner, J. D. (1979) *Biochim. Biophys. Acta 576,* 479−495.
Tokutomi, S., Mizutani, Y., Anni, H., & Kitagawa, T. (1990) *FEBS Lett. 269,* 341−344.
Tokutomi, S., Sugimoto, T., & Mimuro, M. (1992) *Photochem. Photobiol. 56,* 545−552.
Toyama, A., Nakazawa, M., Manabe, K., Takeuchi, H., & Harada, I. (1993) *Photochem. Photobiol. 57,* 391−395.
Vierstra, R. D., & Quail, P. H. (1986) *Photomorphogenesis in Plants* (Kendrick, R. E., & Kronenberg, G. H. M., Eds.) pp 35−60, Martinus Nijhoff, Dordrecht.
Warshel, A., & Karplus, M. (1974) *J. Am. Chem. Soc. 96,* 5677−5689.
Zhang, C.-F., Farrens, D. L., Gjorling, S. C., Song, P.-S., & Kliger, D. S. (1992) *J. Am. Chem. Soc. 114,* 4569−4580.

BI962175K